Aerosol and Air Quality Research, 15: 2654–2667, 2015

ISSN: 1680-8584 print / 2071-1409 online
doi: 10.4209/aaqr.2015.08.0489

Emission of PAHs from a Single Hydrogen-Oxygen PEM Fuel Cell: In Relation to Fuel Cell Carbon Materials

Kuo-Lin Huang[1*], Tsung-Hsuan Tsai[1], Jen-Hsiung Tsai[1], Shui-Jen Chen[1], Wen-Jhy Lee[2]

[1] *Department of Environmental Engineering and Science, National Pingtung University of Science and Technology, Neipu, Pingtung 91201, Taiwan*
[2] *Department of Environmental Engineering, National Cheng Kung University, Tainan City, 70101, Taiwan*

ABSTRACT

This study investigates the emissions of polycyclic aromatic hydrocarbons (PAHs) from a single hydrogen-oxygen proton exchange membrane (PEM) fuel cell (FC) and its relation to FC carbon materials. The results show that the magnitude of specific areas or pore volumes followed the order BP2000 > XC-72R > XC-72 > Alfa for carbon blacks and multi-walled carbon nanotube (MWCNT) > single-walled carbon nanotube (SWCNT) for CNTs.

Nap and high carcinogenic potency species (BaP, DBA, and IND) were dominant in almost all tested carbon materials (carbon black, CNT, carbon cloth (CC), waterproof CC (WPCC), and waterproof carbon paper (WPCP), except mesophase graphite powder (MGP)). Of all the tested carbon materials, both SWCNT and MWCNT showed the (same) highest BaP content (67.0 μg g^{-1}). Similar 21-PAH concentration profiles were observed for XC-72 vs. XC-72R, SWCNT vs. MWCNT, or CC vs. WPCC, consistent with the results of cluster analysis. The results of the principle component analysis (PCA) showed that two main factors were responsible for the 21-PAH concentration profiles. The Total-PAHs content of the tested carbon materials ranged from 2573 ± 333 (MGP) to 10.2 ± 0.51 (WPCP) μg g^{-1}, while their Total-BaP_{eq} values were in the order MWCNT (155 ± 3.61 μg g^{-1}) ≈ SWCNT >> WPCC > MGP > Alfa ≈ XC-72 > XC-72R >> CC > BP2000 ≈ WPCP (1.13 ± 0.01 μg g^{-1}). The emission concentrations of Total-PAHs were lower from the anode (gas emission: 4360 ± 72 ng Nm^{-3} and water effluent: 277 ± 79 ng L^{-1}) than from the cathode (gas emission: 6904 ± 443 ng Nm^{-3} and water effluent: 572 ± 104 ng L^{-1}). Likewise, the Total-BaP_{eq} concentration (dominated by 5/6/7-ring PAHs) was also lower in anode (640 ± 2.07 ng Nm^{-3}) than in cathode gas emissions (967 ± 8.02 ng Nm^{-3}); however, those in the anode and cathode water effluents were similar (5.70 ± 5.64 and 5.60 ± 4.88 ng L^{-1}, respectively). Accordingly, the H_2-O_2 PEMFC is not a complete zero-emission power generator when considering its PAH emissions during operation.

Keywords: Toxic air pollutant; Polycyclic aromatic hydrocarbon; Carbon nanostructured material; Proton exchange membrane fuel cell.

INTRODUCTION

Polycyclic aromatic hydrocarbons (PAHs) and their derivatives are mostly released into the environment due to incomplete combustion of organic materials as part of various human activities, or from sources such as carbon black manufacturing (Tsai *et al.* 2001), scrap tire pyrolysis (Chen *et al.*, 2007), traffic (Lin *et al.*, 2008), diesel generators (Chen *et al.*, 2012), smoldering incense (Yang *et al.*, 2013), plasma-enhanced combustion (Lin *et al.*, 2013), coal-fired plants (Li *et al.*, 2014), and coal/sludge co-combustion (Chen *et al.*, 2014). PAHs have been extensively studied to understand their distribution, fate and effects in the environment (Baek *et al.*, 1991; Kim *et al.*, 2013; Stogiannidis and Laane, 2015), and the PAHs emitted from stationary/mobile sources and present in the air have long been a concern with regard to their adverse health effects, regardless of their sources (Kim *et al.*, 2013). Many developed countries have thus passed much tighter legislation concerning the allowable concentrations of PAHs (especially benzo[a] pyrene (BaP)) in the air, as well as banned the practice of uncontrolled burning, and such actions have reduced the presence of these compounds in ambient air (Kim *et al.*, 2013).

However, little attention has been paid to the PAH emissions from hydrogen-oxygen proton exchange membrane fuel cells (PEMFCs), particularly hydrogen-oxygen (H_2-O_2) PEMFC, which has been hailed for having zero-emission of pollutants and CO_2. PEMFCs are promising alternative power sources for stationary and mobile applications (Wang *et al.*, 2006). The major components of a H_2-O_2 PEMFC

* Corresponding author.
Tel.: +886-8-7703202 ext. 7092; Fax: +886-8-7740256
E-mail address: huangkL@mail.npust.edu.tw

include the membrane-electrode assembly (MEA), bipolar/end plate and gas-diffusion layer (GDL) (Huang *et al.*, 2006). Being the heart of a H_2-O_2 PEMFC, the MEA generally consists of a PEM (solid electrolyte) and two symmetrical electrodes (anode and cathode). The precious metal catalysts (e.g., Pt) in the anode and cathode are usually supported by carbon powders, such as activated carbon, carbon black, carbon fiber, carbon nanotube (CNT), graphite, and graphitized materials, and carbon is also commonly used in fabricating the bipolar/end plates and the GDLs in PEMFCs (Dicks, 2006; Wissler, 2006). When produced for PEMFC applications, carbon bipolar plates are traditionally made by machining graphite sheets impregnated with polymer resin, while the GDL is usually carbon (fiber) paper (CP) or carbon cloth (CC), and the macroporous support layer is coated with a thin layer of carbon black mixed with dispersed hydrophobic resin (typically polytetrafluoroethylene (PTFE)) to render it hydrophobic (Dicks, 2006). Recently developed PEMFCs still use carbon materials in the catalyst support and GDL components. For example, Vulcan XC-72 carbon black and MWCNT are needed to fabricate Ni-CNT catalytic nanomaterials for use in an anodic H_2 oxidation reaction (Tran *et al.*, 2015). Although high-temperature PEMFCs have been developed and studied in order to overcome the drawbacks of traditional low-temperature PEMFCs, some preparation methods (spraying and doctor blade coating in particular) for conventional carbon-containing PEM electrodes are still applied for the fabrication of GDEs for high-temperature PEMFCs (Zeis, 2015).

It is necessary to use a high temperature and/or pressure when fabricating the above mentioned PEMFC carbon materials (Dicks, 2006; Wissler, 2006). Carbon black (particle diameter = ~5–10 nm) is also known as channel black, furnace black, lamp black, thermal black and acetylene black, based on the manufacturing method used to produce it (Wissler, 2006). However, carbon black, graphite, CP, CC, or CNT may absorb PAHs during and after their fabrication. Although PAHs find it relatively easier to adsorb on than to desorb from the surface of carbon black (Moninot, 2010), Tsai *et al.* (2001) reported that the averaged Total-PAHs contents of carbon blacks produced at combustion temperatures of 1780°C and 1950°C were 99.0–119 and 30.2–125 μg g^{-1}, respectively. Chen *et al.* (2007) indicated that the carbon blacks formed in the pyrolysis of scrap tires were mainly 2/3/6/7-ring PAHs, and the contents of LMW-, MMW-, and HMW-PAHs were 48, 12, and 240 μg g^{-1}, respectively. Moreover, the adsorption (Yang *et al.*, 2006) and desorption (Yang and Xing, 2007) of PAHs on SWCNTs and MWCNTs has also been observed. It is thus possible that the PAHs adsorbed on PEMFC carbon materials may be desorbed and then emitted during the operation of PEMFCs.

This work tested several commercial carbon materials that are commonly used for PEMFCs, including carbon blacks, nanotubes, and cloth/papers. One type of mesophase graphite material which can be used to prepare carbon black was also examined for comparison purposes. We characterized 21 PAHs in the carbon materials and determined the emissions of PAHs from a PEMFC (single-cell). The distribution patterns (concentration profiles) of PAHs retained by the carbon materials and emitted from the PEMFC were compared and related to each other. The carcinogenic potencies induced by the PAHs (as equivalent BaP concentrations (BaP_{eq})) were also discussed.

MATERIALS AND METHODS

Carbon Materials

The four nano carbon blacks or graphite powders tested in this work were (Vulcan) XC-72/XC-72R (Cabot, supplied from E-TEK), Alfa (acetylene carbon black, Alfa Aesar), and Black Pearls (BP) 2000 (Cabot). Only one type of mesophase graphite powder (MGP) with micrometer sizes (from China Steel Chemical Corp. (CSCC)) was tested. The MGP is one type of precursor used to make carbon blacks. The single- and multi-walled carbon nanotubes (SWCNT (Cat. No. 519308) and MWCNT (Cat. No. 677248), respectively) of interest were also obtained from Aldrich. Two types of carbon cloth with/without water-proof treatment (denoted as WPCC and CC, respectively) and one type of water-proofed carbon paper (WPCP) from Toray were tested and compared. Following the Brunauer-Emmett-Teller (BET) method, the surface areas and pore volumes of different carbon powders were determined using a sorptometer (Beckman, SA3100) at 77 K with N_2 as the adsorbate. The surface morphological characteristics of the carbon powders were examined using field emission scanning electron microscopy (SEM, JSM-6330, JEOL Co.), while the structures of the carbon materials were scanned by X-ray diffractometry (XRD) (Bruker axs/D8 Advance) with Cu K α radiation (scanning rate: 8° 2θ min^{-1}).

Fuel Cell Emission Test and PAH Sampling

A H_2-O_2 PEMFC was used for the PAH emission tests. The PEMFC was a single cell which had a membrane-electrode assembly (MEA) symmetrically sandwiched by Telfon gaskets, carbon (graphite) blocks (with gas flow channel), and copper current collectors (Fig. 1). With a Pt loading of 0.5 mg cm^{-2} for the anode or cathode, E-TEK MEAs (GDL LT 1400-W) were used in the experiments. An MEA consisted of a Nafion-117 membrane (electrolyte), two dispersed catalyst layers, and two gas diffusion layers (GDL) (Fig. 1). The single cell was installed on a standard fuel cell test station that worked at 65°C (80°C and 70°C for the anode and cathode humidifiers, respectively) and 0.6 V for 48 h for PAH collection. Two mass flow controllers were used to control the anode hydrogen and cathode oxygen flow rates of 52 and 35 sccm, respectively, corresponding to 1.5 and 2 times of the stoichiometric requirements for the anode and cathode feeding gases, respectively (Huang *et al.*, 2006). The sampling system was connected to the single cell and simultaneously collected PAHs from the anode and cathode emission ports (Fig. 2). In each sampling, a glass water collector was adopted to collect PEMFC effluent containing water-phase PAHs, and a glass cartridge packed with XAD-16 resin granules and supported by a polyurethane foam (PUF) plug was used to sample the gas-phase PAHs. After the PAH collection, the cell polarization was conducted at the same test conditions.

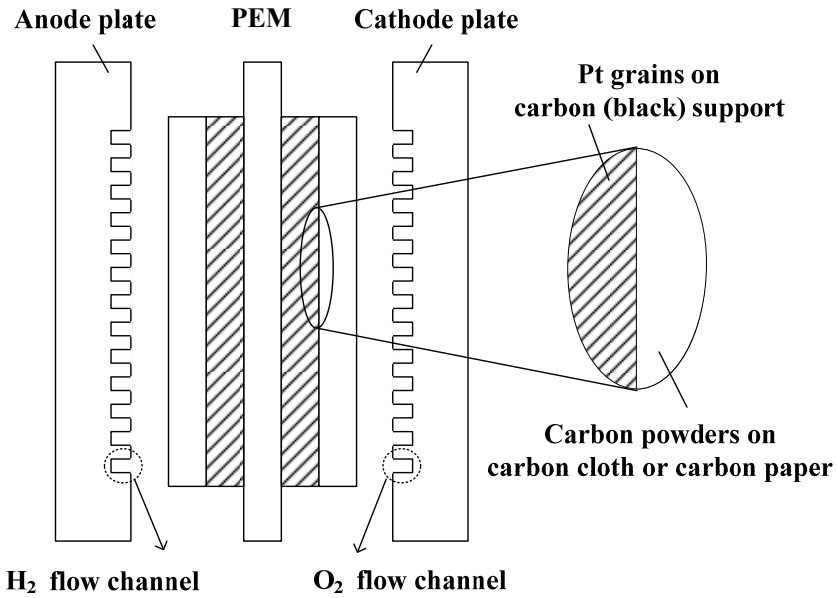

Fig. 1. The single PEMFC with an E-TEK MEA for experiments.

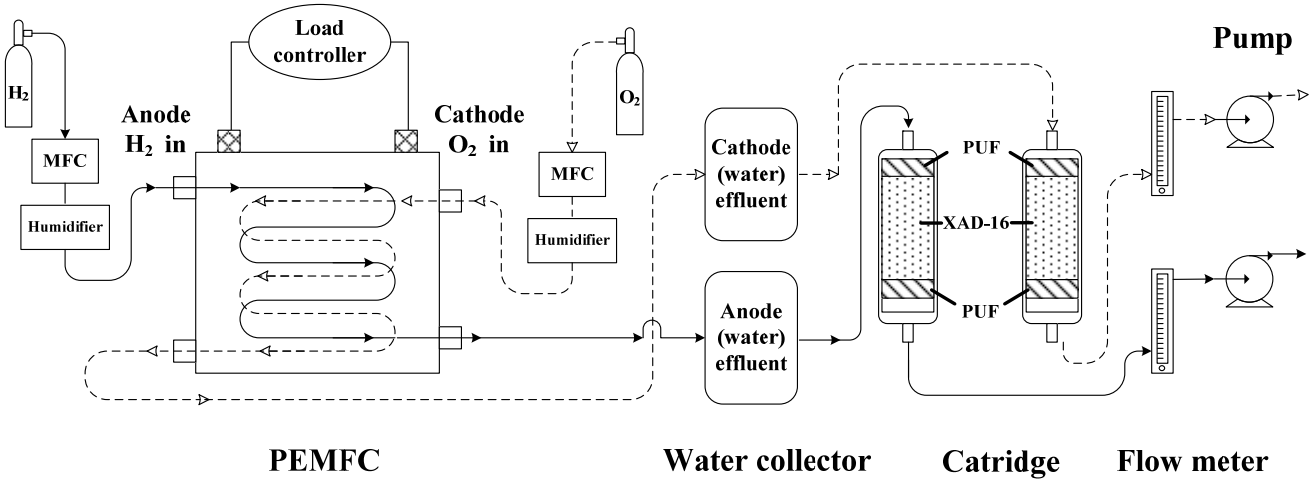

Fig. 2. The sampling device used to collect water- and gas-phase PAHs emitted from the PEMFC.

PAH Analysis and Quality Control

The PAH species determined included one two-ring (Naphthalene (Nap)), five three-ring (Acenaphthylene (AcPy), Acenaphthene (Acp), Fluorene (Flu), Phenanthrene (PA), Anthracene (Ant)), four four-ring compounds (Fluoranthene (FL), Pyrene (Pyr), Benzo(a)anthracene (BaA), Chrysene (CHR)), six six-ring (Cyclopenta(c,d)pyrene (CYC), Benzo(b)fluoranthene (BbF), Benzo(k)fluoranthene (BkF), Benzo(e)pyrene (BeP), Benzo(a)pyrene (BaP), Perylene (PER)), four six-ring (Indeno(1,2,3,-cd)pyrene (IND), Dibenzo(a,h)anthrance (DBA), Benzo(b)chrycene (BbC), Benzo(ghi)perylene (BghiP)) compounds, and one seven-ring (Coronene (COR)) PAH compound.

For PAHs extraction and analysis, each carbon material sample was weighed on an electronic five-digit scale (AND GR-120) and placed into a pre-cleaned thimble that was then extracted in a Soxhlet extraction apparatus. All carbon materials, cell emission gas, and cell effluent samples were extracted in the Soxhlet extraction apparatus for 24 hours with 1:1 (v/v) n-hexane/dichloromethane. The extracts were then concentrated, cleaned via a silica column, and reconcentrated by purging with ultra-pure nitrogen to 1.0 or 0.5 mL prior to analysis. The identification and quantification of PAHs was performed via gas chromatograph/mass spectrometer (GC/MS) measurements using a GC (Hewlett-Packard 5890A) with a Hewlett-Packard capillary column (HP Ultra 2- 50 m × 0.32 mm i.d., 0.17 μm film thickness), and a mass selective detector (MSD) (Hewlett-Packard 5972). The GC/MS instrument was controlled with a computer workstation and equipped with an HP-7673A automatic sampler, and it was operated with the following conditions: injection volume = 1 μL, splitless injection = 300°C, ion source temperature = 310°C; oven heating from 50 to 100°C at 20 °C min^{-1}, 100 to 290°C at 3 °C min^{-1}, and then 290°C -held for 40 min. A scan mode was employed to determine the masses of the molecular and fragment ions

of pure PAH standards in the GC/MS analysis. The quantification of PAHs was performed using the selective ion monitoring (SIM) mode. The system was calibrated with a diluted standard solution containing sixteen PAH compounds (PAH Mixture 610-M from Supelco) plus five individual PAH compounds (from Merck). The response factors of the PAH standard solution were used to calculate the masses of the sampled PAHs at the same GC/MS relative retention time (RRT).

The total-PAHs concentration was regarded as the sum of the concentrations of 21 PAH species for each collected sample. To assess the PAH homologue distribution of each sample, the concentrations of PAH species with low molecular weight (LMW-PAHs, 2-/3-ring PAHs: NaP, AcPy, AcP, Flu, Ant, and PA), middle molecular weight (MMW-PAHs, 4-ring PAHs: FL, Pyr, BaA, and CHR), and high molecular weight (HMW-PAHs, 5-/6-/7-ring PAHs: CYC, BbF, BkF, BeP, BaP, PER, DBA, BbC, IND, BghiP, and COR) were determined.

All PAHs were corrected with procedural blanks that were consistently analyzed with the samples. The PAHs were quantified based on the retention times and areas under the peaks obtained from the calibration standards. At least five standard concentrations, covering the concentrations of interest, were used in PAH analysis calibration. The correlation coefficients of the calibration curves were 0.995–0.999.

Each week the GC/MS was calibrated using a diluted standard solution containing 16 PAH compounds (PAH Mixture-610 M from Supleco), five additional PAHs (Pyr, CYC, BeP, BbC, and COR), purchased from Merck, and five internal standards (Nap-d8, Acp-d10, PA-d10, CHR-d12, and PER-d12) (SRM1597, PolyScience). Ten consecutive injections of a PAH 610-M standard yielded an average relative standard deviation (RSD) of the GC/MS integration area of 3.0% with a range of 0.8–5.1%. The recovery efficiencies of 21 individual PAHs were obtained by experimentally processing a solution with known PAH concentrations in the same way that the samples were processed. Seven consecutive injections yielded total recovery efficiencies of PAHs ranging from 74 to 110%, with an average of 86%. The mean relative standard deviations (RSDs) of the recovery efficiencies were about 17%, and the potential errors in PAH analyses were around 16%. The average recoveries of the five internal standards were 85–93% across seven consecutive injections.

The coefficients of variation for repeat injections of the standard solution (containing PAH Mixture-610 M (16 PAHs) and five Merck PAH standards) were all less than 5% for all of the analyzed PAHs, whereas those obtained by replicate analysis were 2–10%. Analyses of serial dilutions of PAH standards revealed the limits of detection (LODs) of GC/MS to be between 0.010 and 0.474 ng for the 21 PAH compounds. The limit of quantification (LOQ) was defined as the LOD divided by the sampling volume. The LOQ values of the 21 PAH compounds for carbon material, cell emission gas, and cell effluent samples were between 0.008–0.016 ng g^{-1}, 0.076–0.175 ng Nm^{-3}, and 0.102–2.47 ng L^{-1}, respectively.

RESULTS AND DISCUSSION

Characteristics of Carbon Materials

According to SEM examination, the size ranges (30–70 nm) and average particle sizes of XC-72, XC-72R, Alfa, and BP2000 carbon blacks were comparable (Figs. 3(a)–3(d), respectively). The average particle sizes of BP2000 were greater than those observed by Wang *et al*. (2006) and Kinoshita (1988), but similar to the observation of Lavall *et al*. (2008). The diameters (28–70 μm) of mesophase graphite powders (MGPs) were much greater than those of carbon blacks (Fig. 3(e)). As expected, the diameters of single-wall carbon nanotubes (SWCNT) (1.2–1.5 nm) were smaller than those of multi-wall carbon nanotubes (MWCNT) (10–15 nm) (Figs. 3(f) and 3(g), respectively). Among the tested carbon blacks, BP2000 (1444 m^2 g^{-1}) and Alfa (69 m^2 g^{-1}) exhibited the largest and smallest specific areas, respectively; the specific areas of XC-72 and XC-72R were also comparable (227 and 213 m^2 g^{-1}, respectively), and similar to the results reported in the literature (Lasch *et al.*, 2002; de la Fuente *et al.*, 2006). The specific areas of SWCNT (279 m^2 g^{-1}) and MWCNT (260 m^2 g^{-1}) were comparable to those of XC-72 and XC-72R, while that of MGP was quite small (0.631 m^2 g^{-1}) due to its larger particle sizes. The magnitude of pore volume was in the order carbon nanotube > carbon black > MGP. Table 1 summarizes the average particle sizes, specific areas, and porosities of the tested carbon/graphite powders. The appearance of the (carbon fiber) bundles-woven carbon cloth (CC) (Fig. 3(h)) was similar to that of water-proof (PTFE- or Teflon-treated) carbon cloth (WPCC) (Fig. 3(i)); however, the surface of the latter was partially covered by water-proof material. Both the CC and WPCC had similar sizes of threads (5–7 nm) in their bundles, comparable to that (5–10 nm) of water-proof carbon paper (WPCP) (Fig. 3(k)).

In Fig. 4, the XC-72, XC-72R, and Alfa have similar broad XRD peaks centered at 2θ of ~25° corresponding to similar levels of graphitization; on the other hand, this graphitization peak is not so clear for BP2000. A larger degree of graphitization implies a higher carbonization temperature during carbon black preparation, and more graphitized carbon should have higher conductivity, which may increase the electrochemical performance of the electrode (Kim *et al.*, 2007). Compared to the four carbon blacks tested in this work, the MGP and MWCNT had similar sharper and narrower XRD peaks located at 2θ = ~26°, indicating a more ordered graphitic structure (graphite (002)) (Somani *et al.*, 2006; Shanahan *et al.*, 2008). However, the XRD spectrum of SWCNT, different from that of MWCNT, exhibited an intense peak at 2θ = 44.4° (graphite (101)) (Shanahan *et al.*, 2008).

Concentrations and Comparison of PAHs of Carbon Materials

For XC-72, the content (mean of triplicate measurements) of 21 individual PAHs varied from 0.08 to 65 μg g^{-1} and the dominant species were Nap, BaA, BbF, BkF, Bap, IND, DBA, and BghiP (Fig. 5); with similar dominant PAH species, the XC-72R had a PAHs content of 0.06–10.1

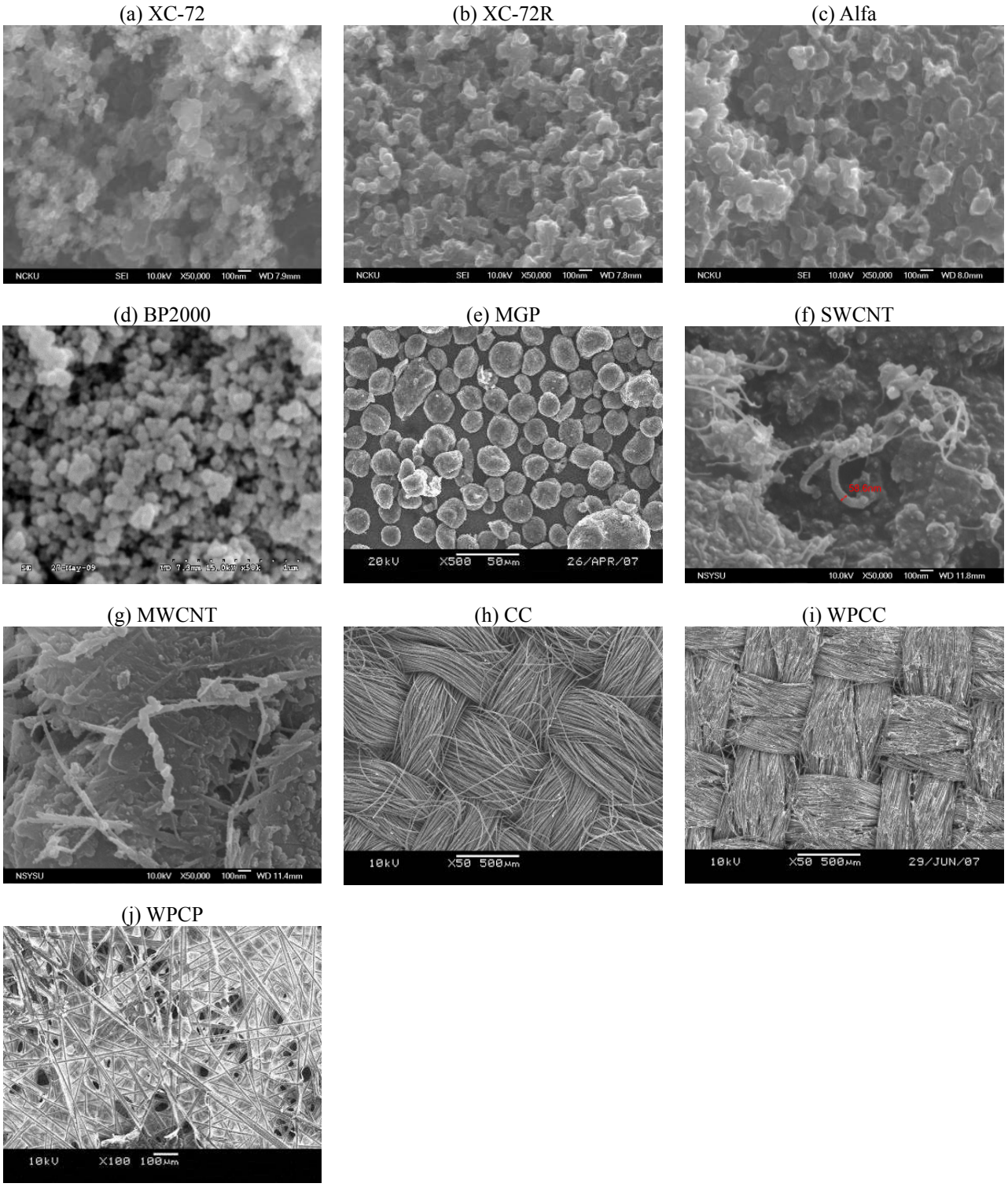

Fig. 3. SEM images of tested PEMFC carbon materials (carbon blacks (XC-72 (a), XC-72R (b), Alfa (c), and BP2000 (d)), mesophase graphite powders (MGPs (e)), single/multi-wall carbon nanotubes (SWCNT (f) and MWCNT (g)), carbon cloth (CC (h)), water-proof (Teflon-treated) carbon cloth (WPCC (i)), and water-proof carbon paper (WPCP (k))).

μg g^{-1}. The PAHs content of Alfa acetylene and BP2000 carbon black grains ranged from ND–25.9 and 0.02–136 μg g^{-1}, respectively. Of all the 21 PAH species, Nap exhibited the highest content for these four types of carbon blacks. A relatively high content of IND was observed for XC-72, XC-72R, and Alfa carbon blacks. This phenomenon was also found for the carbon black in scrap tire pyrolysis (Chen *et al.*, 2007), but not for that in carbon black manufacturing (Tsai *et al.*, 2001). The Total-PAHs contents of the carbon blacks in this study were greater than those observed by

Table 1. Diameters (D_A, nm), specific areas (SA, m^2 g^{-1}), and pore volumes (P, mL g^{-1}) of tested carbon blacks (XC-72, XC-72R, Alfa, and BP2000), mesophase graphite powders (MGPs), and single/multi-wall carbon nanotubes (SWCNT and MWCNT).

	XC-72[I]	XC-72R[II]	Alfa[I]	BP2000[II]	MGP	SWCNT	MWCNT
D_A	30–70 20–50[a]	30–70	30–70 40–42[e]	30–70 12[e]–15[e] 60–70[h]	28–70 μm	5–20 1.2–1.5[i]	5–20 10–15[i,j] 2–6[i,k]
SA	227 250[a] 212[b] 232[$] 223[%]	213 225[c] 203[d] 241[$]	69 62[e] 80[f]	1444 ~1500[e,g,h] 1485[$] 1337[%]	0.631	279	260
P	0.4609 0.68[%]	0.3298	0.1778 0.0045*[e] 0.23**[e]	0.1958* 0.2191*[e] 2.37**[e] 3.06[%]	0.0042	0.8146	0.726

a: Gattia *et al*., 2009; b: Lasch *et al*., 2002; c: Hwang *et al*., 2009; d: Go´mez de la Fuente *et al*., 2006; e: Wang *et al*., 2006; f: from Alfa Aesar; g: Kinoshita, 1988; h: Lavall *et al*., 2008; i: Aldrich; j: tube outside diameter; k: tube inside diameter; $: Carmo *et al*., 2007; %: Lazaro *et al*., 2008; *: *t*-Plot micropore volume; **: meso- and macro-pore volume; I: acetylene black (Wang *et al*., 2006); II: oil-furnace black (Wang *et al*., 2006; Dicks, 2006).

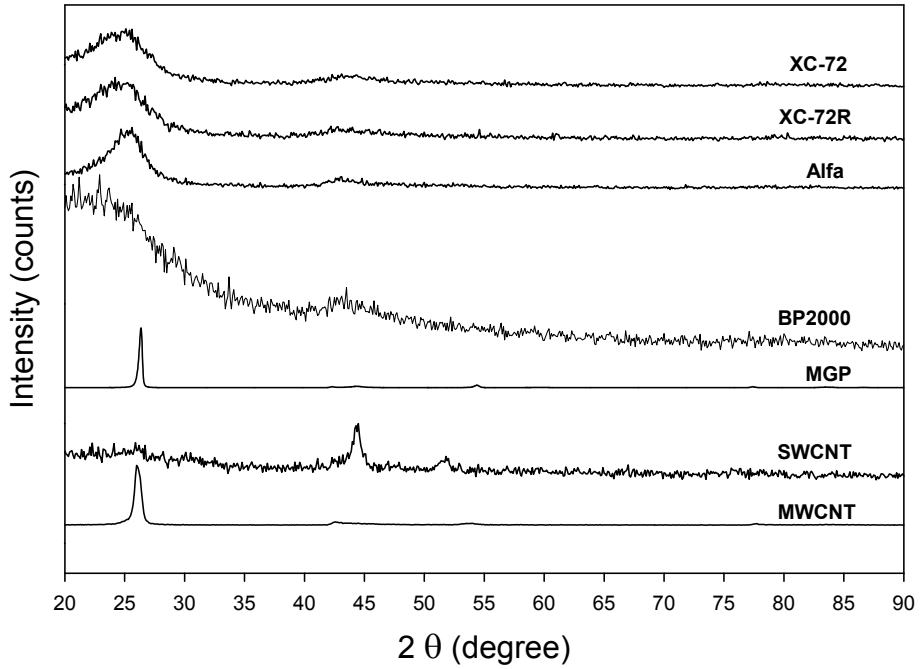

Fig. 4. XRD spectra of tested carbon blacks (XC-72, XC-72R, Alfa, and BP2000), mesophase graphite powders (MGPs), and carbon nanotubes (SWCNT and MWCNT).

Tsai *et al.* (2001). The PAHs content of MGP was in the range 0.02–136 μg g^{-1}. Although the Nap content of MGP was greater than those of the four carbon blacks, the top six dominant PAH species of MGP followed the order PA > Acp > Pyr > Ant > FL > Nap. For SWCNT, MWCNT, CC, WPCC, and WPCP, among 21 PAH species, Nap and IND ranked the first and second highest in content, respectively. Nevertheless, the Nap content of SWCNT and MWCNT (499 and 630 μg g^{-1}, respectively) was much higher than those of CC, WPCC, and WPCP (3.42, 21.9, and 2.37 μg g^{-1}, respectively). Among the tested carbon materials, both SWCNT and MWCNT showed the (same) highest BaP content (67.0 μg g^{-1}), which is of most concern with regard to the carcinogenic potency of PAH species (see more discussion of this in the next section).

As seen in Fig. 5, the 21-PAH distribution pattern (concentration profile (Stogiannidis and Laane, 2015)) of XC-72 was roughly the same as that of XC-72R, but different from those of Alfa and BP2000. The 21-PAH distribution pattern of Alfa was also different to that of BP2000. This finding is also supported by cluster analysis (Statistica 6.0) for the different carbon blacks, based on their 21-PAH

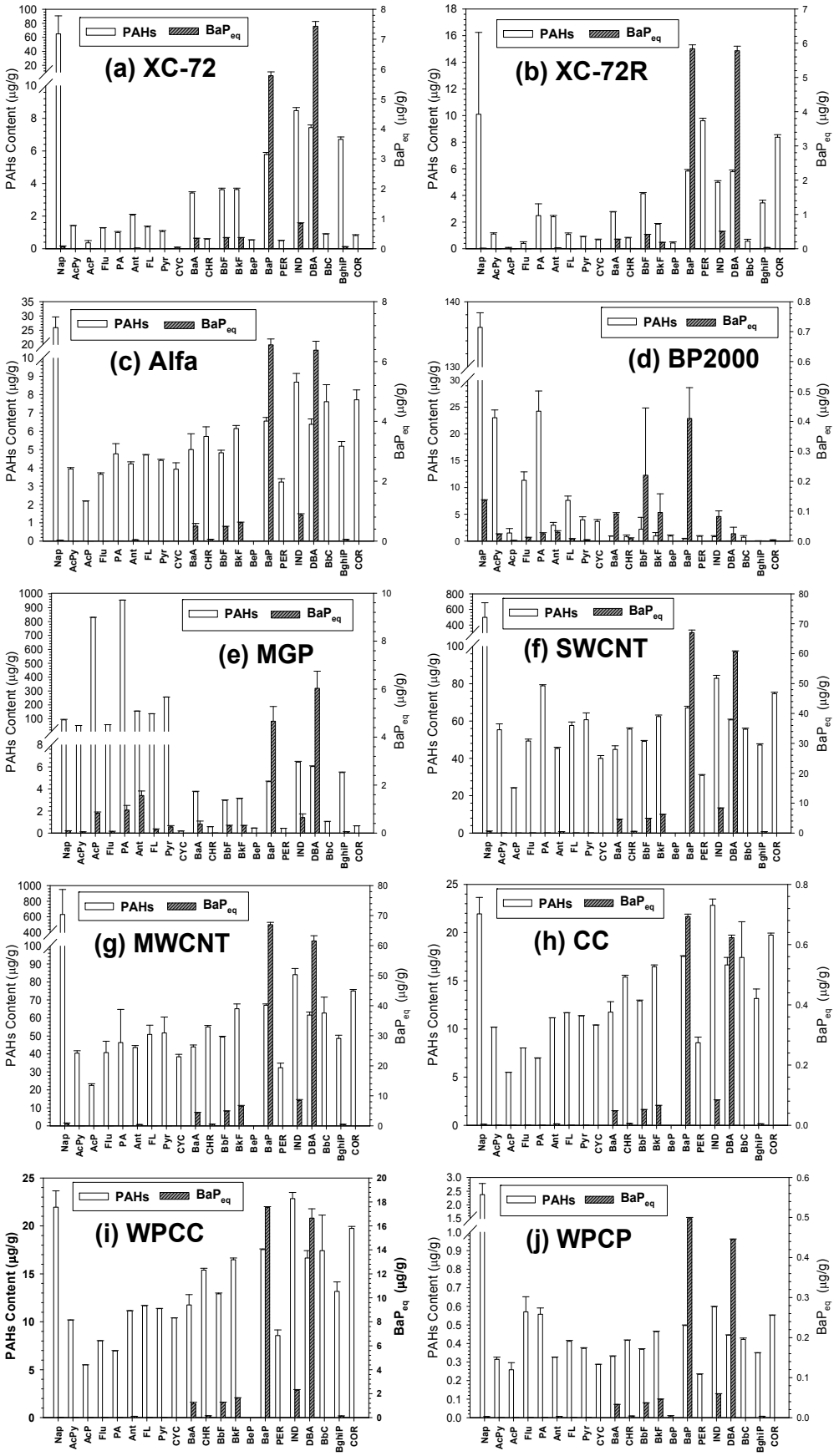

Fig. 5. Characteristic profiles of PAHs and BaP_{eq} of tested PEMFC carbon materials: (a) XC-72, (b) XC-72R, (c) Alfa, (d) BP2000, (e) MGP, (f) SWCNT, (g) MWCNT, (h) CC, (i) WPCC, and (j) WPCP (n = 3).

contents (Fig. 6(a)). Three main clusters were obtained in the cluster analysis. With regard to the similarity in 21-PAH distribution patterns (profiles), the cluster analysis histogram also suggests that XC-72, XC-72R, CC, and WPCP (first cluster) exhibited the highest within-cluster (intra-class) similarity, and this cluster had between-cluster (inter-class) similarity to its neighbor cluster (second cluster) which indicates the within-cluster similarity of XC-72, CC, WPCC, and BP2000. The third cluster with high within-cluster similarity, consisting of SWCNT and MWCNT, showed low between-cluster similarity with regard to the first and second clusters. The between-cluster similarity was even lower between MGP and the second and third clusters. No similarity in 21-PAH distribution patterns was observed between Alfa and MGP or each of the clusters.

The principle component analysis (PCA) found two major factors, Factors 1 and 2, which accounted for 74% and 14% of the total variance, respectively (Fig. 6(b)). Factor 1

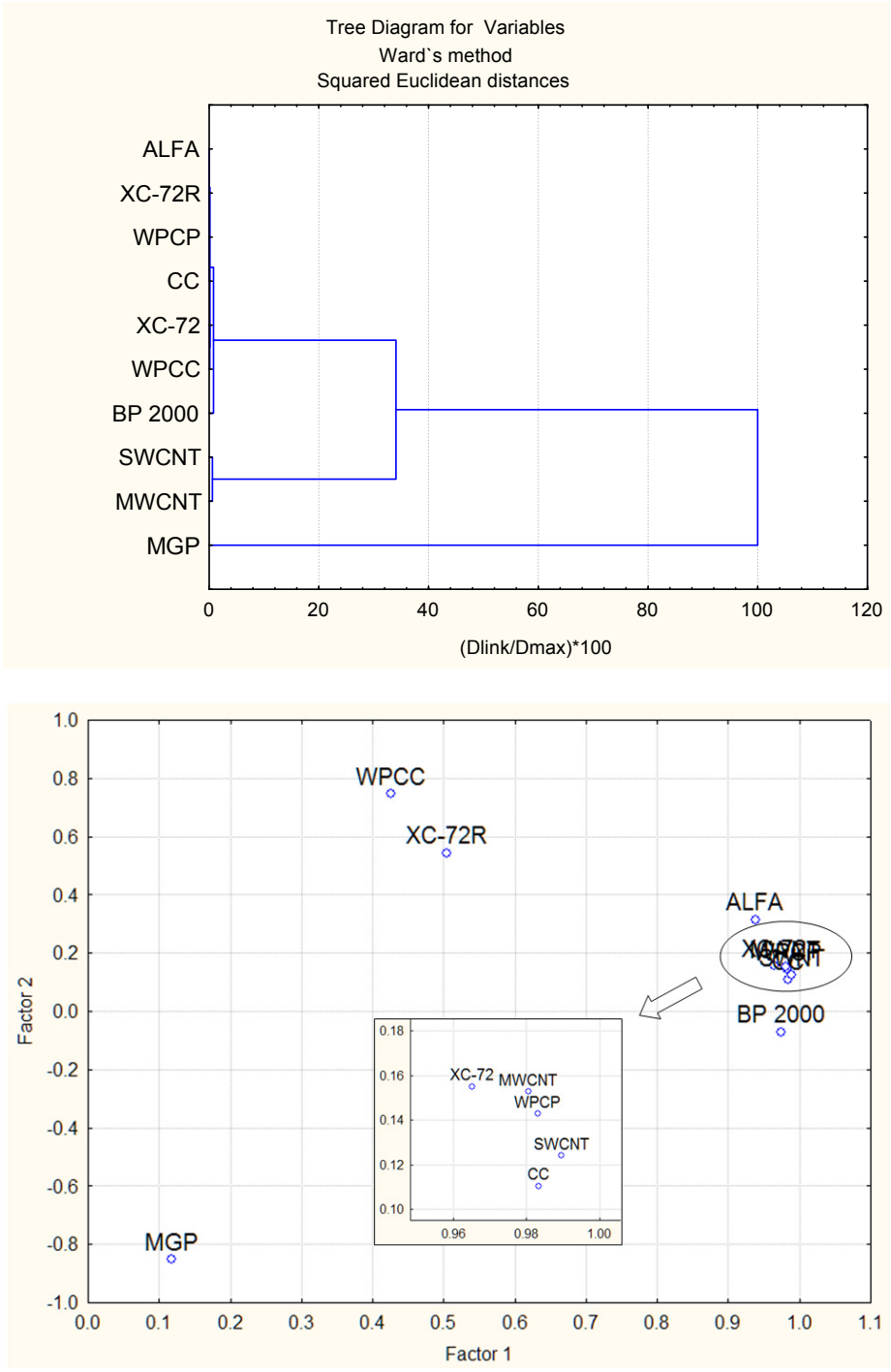

Fig. 6. Cluster Analysis (a) and Principle Component Analysis (b) for the PAHs of tested PEMFC carbon materials; Factors 1 and 2 account for 74% and 14% of total variance, respectively.

was more related to the 21-PAH distribution patterns of XC-72, MWCNT, WPCP, SWCNT, CC, Alfa, and BP2000, whereas Factor 2 showed a closer relation to those of WPCC and XC-72. Factor 1 was slightly responsible for the 21-PAH distribution pattern of MGP, but Factor 2 had a negative relation with it. The PAHs might be generated from pyrogenic, petrogenic, or biogenic/diagenetic sources (Stogiannidis and Laane, 2015). In this study, the 21 PAHs of the tested carbon materials should be attributed chiefly to the pyrogenic source, since these materials are often manufactured in factories. The 21-PAH distribution patterns of the tested carbon materials are generally associated with parameters such as fabrication method, material characteristic, method of PAH adsorption, and so on (Tsai *et al.*, 2001). Suppliers and their different manufacturing methods also influence the carbon blacks' physical (e.g., size, specific area, and pore volume (e.g., size, specific area, and pore volume (Table 1)) and chemical (e.g., graphitization level (Fig. 4)) properties, which may cause the different levels of adsorption of PAHs on the carbon blacks. For example, Yang *et al.* (2006) indicated that different PAHs (Pyr, PA, and Nap) adsorption is related to their molecular size (i.e., the larger the molecular size, the lower the adsorbed volume capacity) and other parameters, whereas different carbon nanomaterials adsorption seems to be related to the surface area, micropore volume, and the volume ratios of mesopores to micropores. Alfa is supplied by Alfa Aesar, while XC-72, XC-72R, and BP2000 are products of Cabot Corporation (Dicks, 2006); furthermore, XC-72, XC-72R, and Alfa are acetylene black, but BP2000 is furnace black (Dicks, 2006; Wissler, 2006). In fact, the only difference between XC-72 and XC-72R is that the former is in the form of pellets (Carmo *et al.*, 2007) or quite-spherical particles (Gattia *et al.*, 2009), whereas the latter is in powder form (Carmo *et al.*, 2007). It is well known that the formation of synthetic carbon black or graphite is greatly dependent on the carbonization temperature (Dicks, 2006; Wissler, 2006). Accordingly, it is possible that Factor 1 was related to the fabrication method (and especially the temperature), while Factor 2 was associated with another fabrication parameter (most likely pressure), the material characteristics, or PAH adsorption.

BaP_{eq} Associated with PAHs in Carbon Materials

The content of total-PAHs of XC-72 reached 116 ± 24.3 μg g^{-1} with the following order: LMM-PAHs > HMM-PAHs > MMM-PAHs, mainly because of the highest content of Nap among the PAH species (Fig. 7(a)). Although XC-72R had dominant PAH species similar to those of XC-72, the content of Nap for XC-72R was only one-sixth that for XC-72 (Figs. 5(a) and 5(b)). As a result, XC-72R had the lowest total-PAHs content (67.8 ± 7.16 μg g^{-1}) with the following order: HMM-PAHs > LMM-PAHs > MMM-PAHs. The total-PAHs content (223 ± 2.87) of BP200 was higher than that of Alfa acetylene black grains (125 ± 1.03 μg g^{-1}) and those of XC-72 and XC-72R. Although varying with the tested carbon materials, the orders of magnitude for LMM-, MMM-, and HMM-PAHs of SWCNT and MWCNT were the same as that of XC-72. A different tendency (LMM-PAHs > MMM-PAHs > HMM-PAHs) was observed for MGP, which had the highest total-PAHs content (2573 ± 333 μg g^{-1}) among the tested carbon materials. For the carbon GDL materials, the total-PAHs content (269 ± 10.3 μg g^{-1}) of WPCC was significantly greater than those of CC and WPCP.

The content of LMM-, MMM-, or HMM-PAHs is regarded as one of two main factors which influence their PAH carcinogenic potency. The other main factor is the structure of the PAH. In general, PAH compounds with more rings, such as BaP, DBA, BaA, BbF, BkF, and IND, are more toxic. The carcinogenic potencies of PAHs can be evaluated by determining their toxic equivalence factors (TEFs) following the conversion of PAH concentration into Benzo(a)pyrene (BaP)-equivalent carcinogenic potency (BaP_{eq}) (Nisbet and LaGoy, 1992).

Fig. 7(b) shows the BaP_{eq} profiles associated with the LMM-, MMM-, HMM-, and Total-PAHs of the tested carbon materials. It is noted that the magnitude of BaP_{eq} values was in the order HMM- >> MMM- > LMM-PAHs for almost all the tested carbon materials, except MGP, with an order HMM- > LMM- > MMM-PAHs in BaP_{eq}, mainly due to the different contents and TEFs, as discussed above. For the tested carbon materials, the magnitude of their BaP_{eq} values followed the order MWCNT (155 ± 3.61 μg g^{-1}) ≈ SWCNT >> WPCC > MGP > Alfa ≈ XC-72 > XC-72R >> CC > BP2000 ≈ WPCP (1.13 ± 0.01 μg g^{-1}). Accordingly, among the tested carbon black materials, the BP2000 had the lowest BaP_{eq} value (1.17 ± 0.26 μg g^{-1}), although it had the highest Nap content. In contrast, of all the tested carbon GDL materials the WPCC exhibited the greatest BaP_{eq} value (41.0 ± 1.06 μg g^{-1}), in accordance with its highest content of MMM-PAHs.

Emissions of PAHs and PAHs-Associated BaP_{eq} from a Single Fuel Cell

The concentration profiles of PAHs emitted from a single fuel cell are shown in Fig. 8. The concentrations of PAHs in anode emission gas ranged from 347 ± 19.6 (Nap) to ND (BeP) ng Nm^{-3} (Fig. 8(a)); for cathode emission gas, the corresponding data were 521 ± 1.30 (IND) to ND (BeP) ng Nm^{-3} (Fig. 8(b)). It is interesting that the concentration profile of PAHs in anode emission gas was similar to that in the cathode emission gas, although the PAH concentration was higher in the anode emission gas than in cathode emission gas for each of the 21-PAH species. This finding is attributable to the greater gas sampling volume for the anode than for the cathode, and the assumption of similar amounts of PAHs emitted from both electrodes. It is also inferred that the emissions of PAHs in anode and cathode gases were influenced by the different operating conditions of these two electrodes. As stated in the Experimental section, the single fuel cell worked at 65°C and anode hydrogen and cathode oxygen flow rates of 52 and 35 sccm, respectively. These two electrodes were also operated at different potentials (anode: < 1.23 V (theoretical) vs. standard hydrogen electrode (SHE); cathode: ~0 V vs. SHE) with different electrochemical reactions (anodic hydrogen oxidation ($H_2 \rightarrow 2H^+ + 2e^-$) and cathodic oxygen reduction ($2H^+ + 2e^- + 1/2O_2 \rightarrow H_2O$),

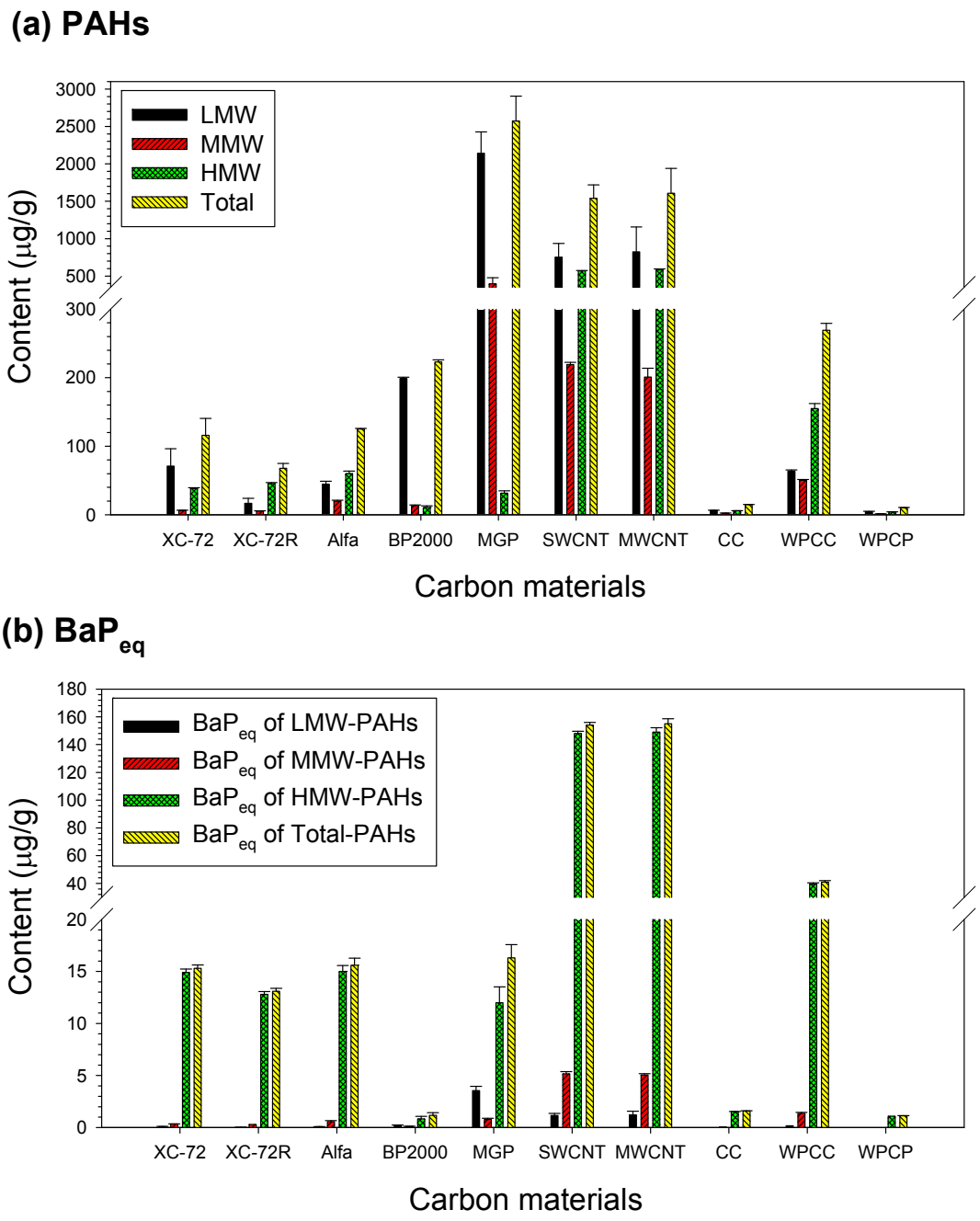

Fig. 7. LMM-, MMM-, HMM-, and Total-PAHs (a) and corresponding BaP_{eq} (b) of tested PEMFC carbon materials (n = 3).

respectively). Moreover, more water was present on the cathode side than on the anode side because of the product (water) generated from the mentioned oxygen reduction reaction, regardless of the different operating temperatures of the anode and cathode humidifiers (80°C and 70°C, respectively). The concentration profiles of the PAHs in the anode or cathode emission gas were more similar to those of Alfa, SWCNT, MWCNT, CC, or WPCC than those of XC-72, XC-72R, or WPCP. In this study, the MEAs from E-TEK consisted of a Nafion-117 membrane (electrolyte), two dispersed catalyst layers (Pt on carbon black support), and two GDLs (Fig. 1); furthermore, Vulcan XC-72 and XC-72R are commonly used in E-TEK MEAs (Dicks, 2006; Lavall *et al.*, 2008; Hwang *et al.*, 2009). Therefore, the PAHs in the anode or cathode emission gas should be associated with the desorption of the PAHs adsorbed on the carbon black and GDL materials (not just the former) during the operation of the PEMFC.

It is known that three phases (gas, liquid, and solid) coexist in the anode or cathode reaction zone on the surface of the carbon materials in a PEMFC. The water from the humidification and reaction might thus affect the PAHs desorption from the carbon materials and the PAHs emission from the sampling anode and cathode gases and water effluents. The concentrations of PAHs in the anode water effluent were in the range 187 ± 60 (Nap) to ND (BkF, BeP,

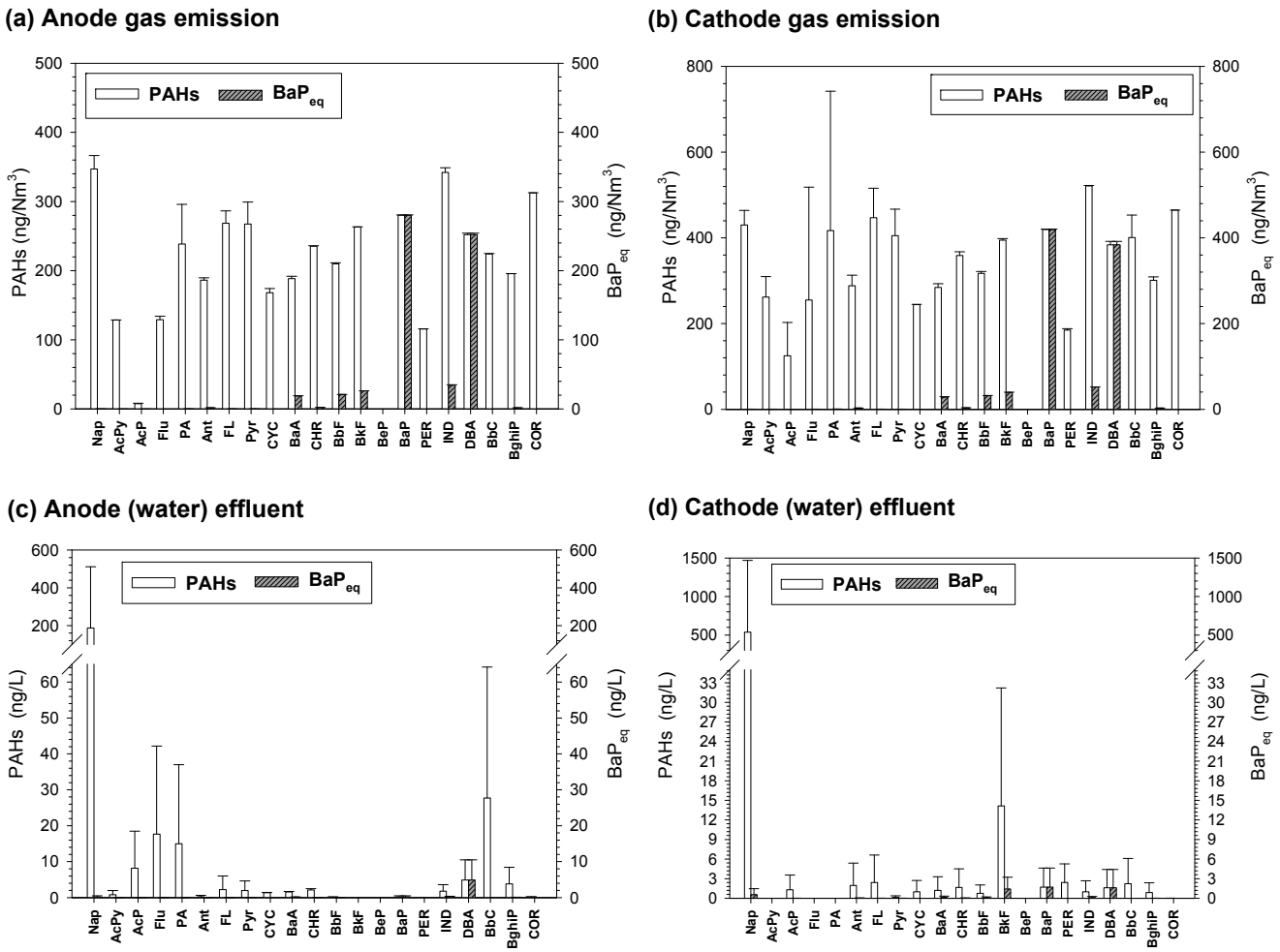

Fig. 8. Characteristic profiles of PAHs and BaP_{eq} emitted from the PEMFC (n = 3) ((a) and (b): anode and cathode gas emissions, respectively; (c) and (d): anode and cathode water effluents, respectively).

and PER) ng L^{-1} (Fig. 8(c)), while in cathode water effluent the corresponding data were 538 ± 100 to ND (Flu, PA, and BeP) ng L^{-1} (Fig. 8(d)). The similarity of the PAHs profiles for anode vs. cathode water effluents was lower than that seen for anode vs. cathode gas emissions. Moreover, the PAHs profiles of the anode and cathode water effluents were not similar to those of the anode and cathode gas emissions. Again, this phenomenon is likely to be associated with the desorption of PAHs from the tested carbon materials in contact with the three-phase zone. Yang and Xing (2007) also observed desorption hysteresis of PAHs (Pyr, PA, and Nap) for fullerene but not for SWCNTs and SWCNTs in water, and the potential release of PAHs in aqueous environment due to the reversible adsorption of PAHs on CNTs, although the graphitic structure of CNTs might have strong interactions with PAHs through π-π interactions (Kah *et al.*, 2011).

In the anode and cathode gas emissions the concentrations of Total-PAHs were 4360 ± 72 and 6904 ± 443 ng Nm^{-3}, respectively (Fig. 9(a)), while those in anode and cathode water effluents were 277 ± 79 and 572 ± 104 ng L^{-1}, respectively (Fig. 9(b)). Both the anode and cathode gas emissions exhibited different concentrations of molecular-weight classified PAHs with the following order: LMM- < MMM- < HMM-PAHs; consequently, their PAH-derived BaP_{eq} values also followed this order in magnitude with Total-BaP_{eq} data of 640 ± 2.07 and 967 ± 8.02 ng Nm^{-3}, respectively. However, LMM-PAHs dominated the Total-PAHs in the anode and cathode water effluents, and thus their PAH-derived BaP_{eq} values were in the order MMM- < LMM- < HMM-PAHs, with Total-BaP_{eq} values of 5.70 ± 5.64 and 5.60 ± 4.88 ng L^{-1}, respectively. Accordingly, the Total-BaP_{eq} was contributed principally by HMM-PAHs, regardless of the difference in gas emissions or water effluents. The BaP_{eq} derived from PAH species (BaP and DBA) with the highest TEF was more predominant in the gas emissions than in the water effluents.

In December 2013, the European Commission issued Regulation No 1272/2013 limiting the content of eight PAHs (EU-8 PAHs) in plastic or rubber parts (usually made from carbon black). To meet this regulation, in June 2015 Cabot Corp. launched a new series of low PAH carbon black products for rubber product applications (Cabot Corp., 2015). According to the Global Automotive Declarable Substance List (GADSL), the PAH limits arbitrarily set on automotive parts made from carbon black are the sum of EU-8 PAHs <

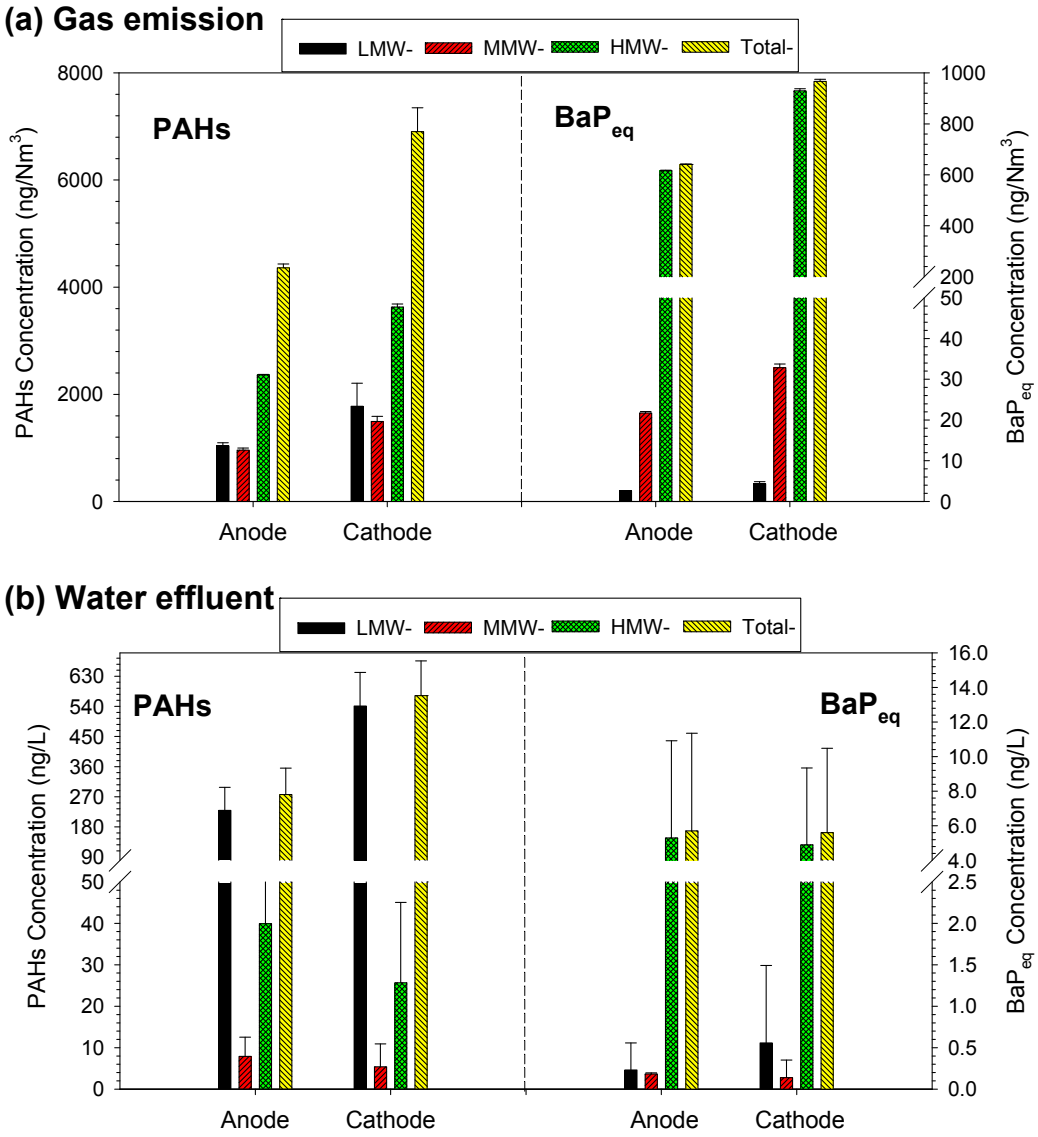

Fig. 9. LMM-, MMM-, HMM-, and Total-PAHs and corresponding BaP_{eq} emitted from the PEMFC (n = 3) ((a) and (b): gas emissions and water effluents, respectively).

200 ppm and BaP < 20 ppm in polymers (Moninot, 2010). Accordingly, it is suggested that the regulation of PAHs of PEMFC carbon materials or their finished articles/products should be considered.

CONCLUSIONS

In this study it is concluded that the specific areas or pore volumes of the four tested carbon blacks varied with the order BP2000 > XC-72R > XC-72 > Alfa (regardless of similar particle size ranges); MWCNT > SWCNT for carbon nanotubes; and MGP had the smallest specific area and pore volume due to its largest particle size among the tested carbon materials. Similar graphitic structures were observed for XC-72, XC-72R, and Alfa, as well as between MGP and MWCNT.

Among the 21 PAH species, Nap exhibited the highest content for the four types of carbon blacks; for SWCNT, MWCNT, CC, WPCC, and WPCP, the PAH species with the first and second highest contents were Nap and IND, respectively, while for MGP they were PA and AcP, respectively. Of all the tested carbon materials, both SWCNT and MWCNT showed the (same) highest BaP content (67.0 μg g^{-1}). The 21-PAH concentration profile of XC-72 was approximately the same as that of XC-72R, but different from those of Alfa and BP2000. The 21-PAH distribution pattern of Alfa was also different from that of BP2000. Similar 21-PAH concentration profiles were found for SWCNT vs. MWCNT and CC vs. WPCC. According to the cluster analysis of PAH concentrations, within-cluster similarity was observed for the cluster of XC-72, XC-72R, CC, and WPCP, which exhibited between-cluster similarity to another cluster (SWCNT and MWCNT). The results of principle component analysis (PCA) showed that Factors 1 and 2 accounted for 74% and 14% of total variance, respectively. The former was more related to the 21-PAH

concentration profiles of XC-72, MWCNT, WPCP, SWCNT, CC, Alfa, and BP2000, whereas the latter showed a closer relation to those of WPCC and XC-72. For both cluster and principle component analyses, the 21-PAH concentration profile of MGP was significantly different from those of the other tested carbon materials. The content of the total-PAHs of the tested carbon materials varied from 2573 ± 333 (MGP) to 10.2 ± 0.51 (WPCP) μg g^{-1}, while their BaP_{eq} values followed the order MWCNT (155 ± 3.61 μg g^{-1}) ≈ SWCNT >> WPCC > MGP > Alfa ≈ XC-72 > XC-72R >> CC > BP2000 ≈ WPCP (1.13 ± 0.01 $\mu g^{-1} g^{-1}$).

In anode and cathode gas emissions, the concentrations of Total-PAHs (both dominated by HMM-PAHs) were 4360 ± 72 and 6904 ± 443 ng Nm^{-3}, respectively, while those (dominated by LMM- PAHs) in the anode and cathode water effluents were 277 ± 79 and 572 ± 104 ng L^{-1}, respectively. The concentrations of PAHs-derived BaP_{eq} (dominated by HMM-PAHs) in the anode and cathode gas emissions were 640 ± 2.07 and 967 ± 8.02 ng Nm^{-3}, respectively; the corresponding data (also dominated by HMM-PAHs) in the anode and cathode water effluents were 5.70 ± 5.64 and 5.60 ± 4.88 ng L^{-1}, respectively. The BaP_{eq} derived from PAH species (BaP and DBA) with the highest TEF was more predominant in the gas emissions than in the water effluents. This study thus demonstrates that the H_2-O_2 PEMFC is not a complete zero-emission power generator due to operational PAH emissions. The regulation of the PAHs of PEMFC carbon materials should therefore be considered, because PEMFCs may become a new and non-negligible PAHs emission source when they become commercialized and more widely used in the near future.

ACKNOWLEDGEMENT

The authors would like to thank the Ministry of Science and Technology, Taiwan, R.O.C. for financially supporting this research under Grant No. NSC 96-2211-E-020-011-MY2.

REFERENCES

Baek, S.O., Field, R.A., Goldstone, M.E., Kirk, P.W., Lester, J.N. and Perry, R. (1991). A Review of Atmospheric Polycyclic Aromatic Hydrocarbons: Sources, Fate and Behavior. *Water Air Soil Pollut.* 60: 273–300.

Cabot Corp. (2015). Cabot Launches New Series of Low Polycyclic Aromatic Hydrocarbons (PAH) Carbon Black Products for Rubber Product Applications, http://www.businesswire.com/news/home/20150629005040/en/Cabot-Launches-Series-Polycyclic-Aromatic-Hydrocarbons-PAH, Last Access: Aug. 2015.

Carmo, M., dos Santos, A.R., Poco, J.G.R. and Linardi, M. (2007). Physical and Electrochemical Evaluation of Commercial Carbon Black as Electrocatalysts Supports for DMFC Applications. *J. Power Sources* 173: 860–866

Chen, S.J., Su, H.B., Chang, J.E., Lee, W.J., Huang, K.L., Hsieh, L.T., Huang, Y.C., Lin, W.Y. and Lin, C.C. (2007). Emissions of Polycyclic Aromatic Hydrocarbons (PAHs) from the Pyrolysis of Scrap Tires. *Atmos. Environ.* 41: 1209–1220.

Chen, W.H., Han, J., Qin, L.B. Furuuchi, M. and Mitsuhiko, H. (2014). The Emission Characteristics of PAHs during Coal and Sewage Sludge Co-Combustion in a Drop Tube Furnace. *Aerosol Air Qual. Res.* 14: 1160–1167.

de la Fuente, J.L.G., Rojas, S., Martinez-Huerta, M.V., Terreros, P., Pena, M.A. and Fierro, J.L.G. (2006). Functionalization of Carbon Support and Its Influence on the Electrocatalytic Behaviour of Pt/C in H_2 and CO Electrooxidation. *Carbon* 44: 1919–1929.

Dicks, A.L. (2006). The Role of Carbon in Fuel Cells. *J. Power Sources* 156: 128–141.

Gattia, D.M., Antisari, M.V., Giorgi, L., Marazzi, R., Piscopiello, E., Montone, A., Bellitto, S., Licoccia, S. and Traversa, E. (2009). Study of Different Nanostructured Carbon Supports for Fuel Cell Catalysts. *J. Power Sources* 194: 243–251.

Huang, K.L., Lai, Y.C. and Tsai, C.H. (2006). Effects of Sputtering Parameters on The performance of Electrodes Fabricated for Proton Exchange Membrane Fuel Cells. *J. Power Sources* 156: 224–231.

Hwang, J.Y., Chatterjee, A., Shen, C.H., Wang, J.H., Sun, C.L., Chyan, O., Chen, C.W., Chen, K.H. and Chen, L.C. (2009). Mesoporous Active Carbon Dispersed with Ultra-fine Platinum Nanoparticles and Their Electrochemical Properties. *Diamond Relat. Mater.* 18:303–306.

Kah, M., Zhang, X., Jonker, M.T. and Hofmann, T. (2011) Measuring and Modeling Adsorption of PAHs to Carbon Nanotubes over a Six Order of Magnitude Wide Concentration Range. *Environ. Sci. Technol.* 45: 6011–6017.

Kim, K.H. Jahan, S.A., Kabir, E. and Brown, R.J.C. (2013). A Review of Airborne Polycyclic Aromatic Hydrocarbons (PAHs) and Their Human Health Effects. *Environ. Int.* 60: 71–80.

Kinoshita, K. (1988). *Carbon: Electrochemical and Physicochemical Properties*, First ed., John Wiley & Sons, New York, pp. 1–85.

Lasch, K., Hayn, G., Jo¨rissen, L., Garche, L. and Besenhardt, O. (2002). Mixed Conducting Catalyst Support Materials for the Direct Methanol Fuel Cell. *J. Power Sources* 105: 305c310.

Lavall, R.L., Borges, R.S., Calado, H.D.R., Welter, Cezar., Trigueiro, J.P.C., Rieumont, J., Neves, B.R.A. and Silva, G.G. (2008). Solid State Double Layer Capacitor Based on a Polyether Polymer Electrolyte Blend and Nanostructured Carbon Black Electrode Composites. *J. Power Sources* 177: 652–659.

Lazaro, M.J., Pinilla, J.L., Suelves, I. and Moliner, R. (2008). Study of the Deactivation Mechanism of Carbon Blacks Used in Methane Decomposition. *Int. J. Hydrogen Energy*33: 4104–4111.

Li, H., Liu, G. and Cao, Y. (2014). Content and Distribution of Trace Elements and Polycyclic Aromatic Hydrocarbons in Fly Ash from a Coal-Fired CHP Plant. *Aerosol Air Qual. Res.* 14: 1179–1188.

Lin, C.C., Chen, S.J., Huang, K.L., Lee, W.J., Lin, W.Y., Tsai, J.H. and Chaung, H.C. (2008). PAHs, PAH-induced Carcinogenic Potency, and Particle-extract-induced

Cytotoxicity of Traffic-related Nano/Ultrafine Particles. *Environ. Sci. Technol.* 42: 4229–4235.

Lin, Y.C., Yang, P.M. and Chen, C.B. (2013). Reducing Emissions of Polycyclic Aromatic Hydrocarbons and Greenhouse Gases from Engines Using a Novel Plasma-Enhanced Combustion System. *Aerosol Air Qual. Res.* 13: 1107–1115.

Moninot, G. (2010). Where are the PAHs in the Carbon Black? www.iom3.org/fileproxy/331784, Last Access: Aug. 2015.

Nisbet, C. and LaGoy, P. (1992). Toxic Equivalency Factors (TEFs) for Polycyclic Aromatic Hydrocarbons (PAHs). *Regul. Toxicol. Pharm.* 16: 290–300.

Park, Y.K., Kim, W. and Jo, Y.M. (2013). Release of Harmful Air Pollutants from Open Burning of Domestic Municipal Solid Wastes in a Metropolitan Area of Korea. *Aerosol Air Qual. Res.* 13: 1365–1372.

Shanahan, P.V., Xu, L.B., Liang, C.D., Waje, M., Dai, S. and Yan, Y.S. (2008). Graphitic Mesoporous Carbon as a Durable Fuel Cell Catalyst Support. *J. Power Sources* 185: 423–427.

Somani, P.R., Somani, S.P. and Umeno, M. (2006). Planer Nano-graphenes from Camphor by CVD. *Chem. Phys. Lett*. 430: 56–59.

Stogiannidis, E. and Laane, R. (2015). Source Characterization of Polycyclic Aromatic Hydrocarbons by Using Their Molecular Indices: An Overview of Possibilities, Vol. 234, In *Reviews of Environmental Contamination and Toxicology*, Whitacre, D.M. (Ed.) Springer International Publishing, Switzerland, p. 56–72.

Tran, P.D., Morozan, A., Archambault, S., Heidkamp, J., Chenevier, P., Dau, H., Fontecave, M., Martinent, A., Jousselme B. and Artero, V. (2015). A Noble Metal-free Proton-exchange Membrane Fuel Cell Based on Bio-inspired Molecular Catalysts. *Chem. Sci.* 6: 2050–2053.

Tsai, J.H., Chen, S.J., Huang, K.L., Lin, T.C., Chaung, H.C., Chiu, C.H., Chiu, J.Y., Lin, C.C. and Tsai, P.Y. (2012). PM, Carbon, PAH, and Particle-Extract-Induced Cytotoxicity Emissions from a Diesel Generator Fueled with Waste-Edible-Oil-Biodiesel. *Aerosol Air Qual. Res.* 12: 843–855.

Tsai, P.J., Shieh, H.Y., Hsieh, L.T. and Lee, W.J. (2001). The Fate of PAHs in the Carbon Black Manufacturing Process. *Atmos. Environ.* 35: 3495–3501.

Wang, X., Zhang, H., Zhang, J., Xu, H., Zhu, X.B., Chen, J. and Yi, B.L. (2006). A Bi-functional Micro-porous Layer with Composite Carbon Black for PEM Fuel Cells. *J. Power Sources* 162: 474–479.

Wissler, M. (2006). Graphite and Carbon Powders for Electrochemical Applications. *J. Power Sources* 156: 142–150.

Yang, K., Zhu, L. and Xing, B. (2006). Adsorption of Polycyclic Aromatic Hydrocarbons by Carbon Nanomaterials. *Environ. Sci. Technol.* 40: 1855–1861.

Yang, K. and Xing, B. (2007). Desorption of Polycyclic Aromatic Hydrocarbons from carbon nanomaterials in Water. *Environ. Pollut.* 145: 529–537.

Yang, T.T., Lin, S.T., Hung, H.F., Shie, R.H. and Wu, J.J. (2013). Effect of Relative Humidity on Polycyclic Aromatic Hydrocarbon Emissions from Smoldering Incense. *Aerosol Air Qual. Res.* 13: 662–671.

Zeis, R. (2015). Materials and Characterization Techniques for High-temperature Polymer Electrolyte Membrane Fuel Cells. *Beilstein J. Nanotechnol.* 6: 68–83.

Received for review, August 6, 2015
Revised, October 6, 2015
Accepted, October 10, 2015